Electroactive phase enhancement in poly(vinylidene fluoride-hexafluoropropylene)/polycarbonate blends by hybrid nanofillers

Torabi, Atefeh; Jafari, Seyed Hassan; Khonakdar, Hossein Ali; Goodarzi, Vahabodin; Yu, Liyun; Skov, Anne Ladegaard

Published in:
Journal of Applied Polymer Science

Link to article, DOI:
10.1002/app.51825

Publication date:
2022

Document Version
Peer reviewed version

Electroactive phase enhancement in poly(vinylidene fluoride-hexafluoropropylene)/polycarbonate blends by hybrid nanofillers

Atefeh Torabi [a, e], Seyed Hassan Jafari [a*], Hossein Ali Khonakdar [b,c], Vahabodin Goodarzi [d], Liyun Yu [e], Anne Ladegaard Skov [e]

[a] School of Chemical Engineering, College of Engineering, University of Tehran, P.O. Box: 11155-4563, Tehran, Iran
[b] Department of Polymer Processing, Iran Polymer and Petrochemical Institute, P. O. Box 14965-115, Tehran, Iran
[c] Leibniz Institute of Polymer Research Dresden, Hohe Straße 6, Dresden D-01069, Germany
[d] Applied Biotechnology Research Center, Baqiyatallah University of Medical Sciences, Tehran, Iran
[e]Danish Polymer Centre, Department of Chemical and Biochemical Engineering, Technical University of Denmark, Lyngby, Denmark

Abstract

Electroactive β phase content of poly(vinylidene fluoride-hexafluoropropylene) (PHP) was enhanced by blending approach with polycarbonate (PC) combined with application of barium titanate– multi-walled carbon nanotubes (BT- MWCNT) hybrid nanofillers to boost the dielectric performance of PHP. The samples were melt-blended at 90/10 and 70/30 wt.% (PHP/PC) in the presence of BT and/or MWCNT. SEM results indicated compatibilization of the structure by adding BT or MWCNT; however, the best refinement in morphology was obtained in (90/10)/1.5/1.5 (PHP/PC)/BT/MWCNT nanocomposite. TEM micrographs illustrated the selective localization of BT at PHP and MWCNT at PC while some of both nanofillers were found at the interphase. FTIR and XRD results depicted the increase in β/α ratio of the nanocomposites with a synergistic effect in (90/10)/1.5/1.5 nanocomposite, attributed to the combined utilization of BT and MWCNT and their selective localization in the PHP/PC immiscible blends. DSC analysis substantiated the nucleating effects of BT and MWCNT and consistency with SEM and TEM observations in nanofillers selective localization. The findings of this work suggest that simultaneous introduction of ceramic and conductive nanofillers with their selective localization in PHP/PC blends is efficacious in improving electroactive phase of composites at low filler content.

Keywords

Poly(vinylidene fluoride-hexafluoropropylene); polycarbonate; carbon nanotube; barium titanate; electroactive nanocomposite

*Corresponding author: (S.H. Jafari) shjafari@ut.ac.ir

1. Introduction

High dielectric constant polymer composites owing to their high permittivity, light weight and good processability are potential materials for many modern applications such as self-powered flexible electronic devices[1], and triboelectric[2] or biomechanical energy harvesters.[3] So, choosing a polymeric matrix with inherent high dielectric constant like poly(vinylidene fluoride) (PVDF) is a major plus. Depending on the processing conditions, this polymer crystallizes in five different conformations; α, β, γ, δ, and ε. The α phase is nonpolar since the net dipole moment of TGTG' (T= trans and G= gauche) conformation is zero but the TTTT conformation in the β phase endows the highest dipole moment and thereby electrical active crystalline phase.[4] As such, it is desirable to increase the amount of β phase and consequently the dielectric constant to make PVDF an asset for high energy density applications. Incorporating hexafluoropropylene (HFP) comonomer with higher spontaneous polarization of C-F dipoles, results in a similar crystalline structure to that of PVDF but with higher piezoelectricity and flexibility.[5],[6] Moreover, compared to PVDF, polyvinylidene fluoride-hexafluoropropylene (PHP) shows lower dielectric loss and higher breakdown strength.[7] Incorporating various ceramic[8] or conductive[9],[10] nanofillers has been extensively studied in the literature in order to improve the relative amount of β phase. Barium titanate (BT) ceramic nanofillers with high dielectric constant improve the dielectric properties of the polymeric matrix[11–15]; however, it is shown that by refining nanofiller size to nanometer scale, its dielectric permittivity drops down due to transition from tetragonal to cubic structure,[16] thus, higher amounts of BT is required to achieve the desirable improvement which negatively affects the dispersion quality, flexibility and mechanical performance of the composite.[9],[11] On the other hand, the dielectric constant of the nanocomposite enhances markedly near the percolation threshold of conductive nanofillers such as carbon nanotubes (CNT), while yet, the increased electrical conductivity reduces the

dielectric strength of the system markedly.[17] To tackle this challenge, using combination of conductive and ceramic nanofillers is proposed. Gerhardt et al. showed synergistic effects of adding BT and multi-wall carbon nanotubes (MWCNT) to PVDF matrix and found that the dielectric properties of the nanocomposites were enhanced by optimizing the charge storage and charge transport behavior of the BT and CNT phase.[18] Developing a high dielectric constant and low percolation threshold nanocomposite involving PVDF/BT-CNT core-shell hybrids formed the central focus of Fan's study in which the author found that by thermal treatment the dielectric constant improved more than three times near the percolation threshold and the β polymorph was doubled at the interface of CNT-PVDF.[19]

It is worth mentioning that the degree of modification in properties by adding nanoparticles strongly depends on the polymer matrix, size, dispersion and distribution[20],[21] of the nanoparticles and interactions of filler–matrix at the interface.[5] The high surface area and large van der Waals forces in CNT result in aggregation in polymeric matrix. Researchers tried to improve the dispersion quality by surface modification, functionalization or acid treatment but such approaches damage the nanotubes and deteriorate their unique properties.[22] Instead, polymer blending helps selective localization of the nanoparticles in the multiphase polymeric matrix and producing nanocomposites at low conductive filler content.[23] Polycarbonate (PC) with high dielectric strength, low dissipation factor, low leakage current and high-volume resistivity is a potential match for PHP.[24] Su et al. found that the percolation threshold of the MWCNT-filled PC/PVDF blends was much less than those of MWCNTs-filled individual polymers because of the selective localization of MWCNTs in the PC phase which was substantiated by scanning electron microscopic (SEM) results. Furthermore, the activation energy of conductive network formation for PC/PVDF/MWCNT was close to that of PC/MWCNT system, which further confirms that MWCNTs were dispersed mostly in the PC phase.[25] In another study, Biswas and coworkers prepared PC/PVDF blend nanocomposites for attenuating microwave radiation in which polyaniline (PANI) modified CNT and Fe_3O_4 were localized in PVDF phase and the surface modified BT in the PC phase. By ordered arrangement of nanofillers in the blends, 90% of the electromagnetic radiation was blocked through a synergistic combination of high relative permittivity (from BT and PANI–MWNT–Fe_3O_4), high relative permeability (PANI–MWNT–Fe_3O_4) and high conductivity.[26] Morphological and electrical conductivity

studies of PC/PVDF/CNT/Clay blend nanocomposites showed that selective localization of CNTs at the blend interface decreased the percolation threshold of the system. Addition of clay and/or CNT changed the morphology from sea-island to quasi co-continuous.[27] CNT, graphene nanoplatelets (GnP) and organo-montmorillonite (15A) individually and simultaneously served as reinforcing fillers to prepare PVDF/PC blend-based nanocomposites. Individual and hybrid fillers localization within the PC domains were substantiated by SEM and TEM observations. Some of the organoclays were located at the interface of PVDF/PC blend to modify the blend morphology. Also, addition of CNT led to the development of a quasi co-continuous PVDF-PC morphology.[28] Therefore, it can be concluded from these studies that the selection of components with different compositions and surface energies is critical in achieving selective localization of nanofillers, the resultant morphology and final properties.

In this study, novel quaternary nanocomposites based on PHP/PC blends containing a combination of MWCNT and BT nanoparticles are processed by a simple melt blending method. The effects of PHPC/PC blend ratio and simultaneous presence of conductive (MWCNT) and ceramic (BT) nanofillers on blend morphology, nanofillers selective localization in the blends, β phase content and crystallization behavior are discussed in details.

2. Materials and methods

Poly(vinylidene fluoride-hexafluoropropylene) (PHP, $\bar{M}_n$ =110000 g mol^{-1}), multi-wall carbon nanotube (MWCNT, mean diameter of 110-170 nm, mean length of 5-9 μm, purity>90%) and barium titanate (BT, dielectric constant of 150, particle size<100 nm, purity≥99%) were purchased from Sigma Aldrich, Germany. Polycarbonate Lexan® 121R (PC, processing temperature= 280-300°C, dielectric constant of 2.7) was obtained from Sabic, Denmark.

2.1. Sample preparation

Dielectric nanocomposites were prepared by a simple one-step melt blending. PHP and PC were dried in a vacuum oven at 100°C overnight before mixing and melt blended at 90/10 and 70/30 weight ratios by micro-compounder (DSM Xplore 15 ml, Netherlands) at 150 rpm, 250°C for 10 minutes. The ternary PHP/PC/BT and PHP/PC/MWCNT nanocomposites

were prepared by adding 3 wt.% (with respect to the whole blend) of BT or MWCNT to the blends, respectively. The quaternary PHP/PC/BT/MWCNT nanocomposites were fabricated by addition of 1.5 wt. % of each BT and MWCNT (with respect to the whole blend) to the PHP/PC blend matrices. The micro-blended samples were shaped into circular discs of 25 mm in diameter by hot pressing at 250°C and 100 MPa for 10 minutes followed by cooling down to room temperature. The samples were named as x/y/m/n representing a blend matrix of PHP/PC at x/y weight ratio containing m and n precents of BT and MWCNT, respectively. Table 1 shows the samples names and specific formulations. Figure 1 shows ternary PHP/PC/BT and PHP/PC/CNT nanocomposites. The average film thickness (0.5 mm) was measured by Mega-Check Pocket digital thickness gauge (LIST-MAGNETIK, Germany).

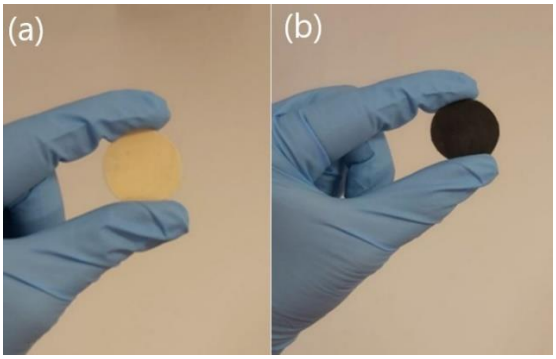

Figure 1. Images of (a) PHP/PC/BT and (b) PHP/PC/CNT nanocomposites

Table 1. Formulation of the test samples

Sample code	**m(PHP) (g)**	**m(PC) (g)**	**m($BaTiO_3$) (g)**	**m(MWCNT) (g)**
100/0/0/0	12.00	-	-	-
0/100/0/0	-	12.00	-	-
90/10/0/0	10.80	1.20	-	-
70/30/0/0	8.40	3.60	-	-
100/0/0/3	11.64	-	-	0.36
90/10/0/3	10.48	1.16	-	0.36

70/30/0/3	8.15	3.49	-	0.36
0/100/0/3	-	11.64	-	0.36
100/0/3/0	11.64	-	0.36	-
90/10/3/0	10.48	1.16	0.36	-
70/30/3/0	8.15	3.49	0.36	-
100/0/1.5/1.5	11.64	-	0.18	0.18
90/10/1.5/1.5	10.48	1.16	0.18	0.18
70/30/1.5/1.5	8.15	3.49	0.18	0.18

2.2. Characterization and measurement of the properties

2.2.1. Rheological measurements

Melt rheological investigations were performed by an oscillatory Discovery series Hybrid Rheometer (DHR-1, TA Instruments) under liquid nitrogen. A parallel plate geometry with 25 mm diameter and 1 mm gap size was used. Prior to the measurement, the samples were melted at 250°C and zero axial force. A strain sweep between 0.1% and 10% was performed to ensure that the measurements were conducted within the linear viscoelastic region. Frequency sweeps from 0.01 to 10 rad s^{-1} and back were accomplished at a temperature of 250°C with an applied strain of 1%.

2.2.2. Scanning electron microscopy (SEM)

The effects of blend ratio and individual or simultaneous presence of BT and MWCNT nanofillers on morphology evolution of the nanocomposites were probed by SEM. The samples were fractured in liquid nitrogen and the gold sputtered cross-section morphology was observed by high-resolution field emission scanning electron microscope ZEISS ultra plus at an accelerating voltage of 20 kV.

2.2.3. Transmission electron microscopy (TEM)

The cross-sectional morphology of the nanocomposites and dispersion quality of nanoparticles were observed with TEM. Sections were cut at -140 °C using a Leica UC7

cryo-microtome with a knife temperature of 30 °C. 80 nm-thin sections were collected on copper grids, then transferred into the Leica FC7 cryo-chamber of the microscope and viewed by LEO 922 OMEGA transmission electron microscope at accelerating voltage of 200 kV. The average diameter of BT nanoparticles was measured by ImageJ software and compared to the reported value by manufacturer.

2.2.4. Fourier transform infrared spectroscopy (FTIR)

To quantitatively follow the changes in the β content by adding BT and/or MWCNT to PHP and/or PHP/PC blends, FTIR analysis was conducted on neat PHP and PC, PHP/PC blends, ternary and quaternary nanocomposites by Thermo Scientific Nicolet iS50 FTIR spectrometer using the Attenuated Total Reflection (ATR) mode. Spectra was acquired in the 400–4000 cm^{-1} range with 32 scans at 4 cm^{-1} resolution.

2.2.5. X-ray diffraction analysis (XRD)

X-ray diffraction (XRD) patterns were obtained by Empyrean multi-purpose diffractometer (Panalytical Empyrean XRD). Nickel filtered CuK_α radiation (λ = 1.5406 °A) operated at accelerating voltage of 40 V and a current of 40 mA served as the source. The patterns were recorded in the 2θ range of 10-50° at a scanning step of 0.02°.

2.2.6. Differential scanning calorimetry (DSC)

DSC as a thermoanalytical technique was used complementary to FTIR and XRD to analyze the crystallinity of the samples. The measurements were performed using a TA Instruments Discovery series differential scanning calorimeter under nitrogen atmosphere from -90 °C to 230 °C at heating or cooling rate of 10 ºC/min. Sample film masses of 2-5 mg were used. Melting temperature (T_m) and enthalpy of fusion (ΔH_m) were calculated from the second heating runs. Crystallization temperature (T_c) and enthalpy of crystallization (ΔH_c) were established from the cooling runs.

3. Results and discussions

3.1. Prediction of nanofillers localization

Localization of a nanofillers in polymer blends can be predicted by Young's equation (Eq. 1) in which ω_a is the wetting coefficient, $\gamma_{filler\text{-}i}$, $\gamma_{filler\text{-}j}$, $\gamma_{j\text{-}i}$ depict the interfacial free energy

between the filler and polymer i, filler and polymer j and polymer i and j, respectively. For ω_a >1, the nanofiller will preferentially locate in the polymer phase nominated j. For -1<ω_a<1, it will localize at the interphase and if ω_a<-1, the filler is predicted to be in the polymer phase denoted i.[29]

$$\omega_a = \frac{\gamma_{filler-i} - \gamma_{filler-j}}{\gamma_{j-i}} \quad \text{(Eq. 1)}$$

Consequently, the wetting coefficients are calculated based on equations 2 and 3 for PHP/PC/BT and PHP/PC/MWCNT, respectively.

$$\omega_a = \frac{\gamma_{BT-PHP} - \gamma_{BT-PC}}{\gamma_{PC-PHP}} \quad \text{(Eq. 2)}$$

$$\omega_a = \frac{\gamma_{MWCNT-PHP} - \gamma_{MWCNT-PC}}{\gamma_{PC-PHP}} \quad \text{(Eq. 3)}$$

The interfacial surface energies between the components are calculated according to theoretical models. Harmonic-mean (Wu's) equation (Eq. 4) is used for low energy materials.[30] while Geometric-mean (Owens-Wendt) equation (Eq. 5) is more suitable for high energy materials.[31]

$$\gamma_{12} = \gamma_1 + \gamma_2 - 4\left[\frac{\gamma_1^d \gamma_2^d}{\gamma_1^d + \gamma_2^d} + \frac{\gamma_1^p \gamma_2^p}{\gamma_1^p + \gamma_2^p}\right] \quad \text{(Eq. 4)}$$

$$\gamma_{12} = \gamma_1 + \gamma_2 - 2(\sqrt{\gamma_1^d \gamma_2^d} + \sqrt{\gamma_1^p \gamma_2^p}) \quad \text{(Eq. 5)}$$

Where γ_i^d, γ_i^p represent dispersive and polar compartment of free surface energy which are assessed by contact angle measurements.[31] These values for PHP, PC, BT and MWCNT are listed in Table 2.

Table 2. Reported values of γ, γ_d and γ_p for PHP, PC, BT and MWCNT at room temperature

Material	$\boldsymbol{\gamma_d}$ **(mN/m)**	$\boldsymbol{\gamma_p}$ **(mN/m)**	$\boldsymbol{\gamma}$ **(mN/m)**	**Reference**
PHP	40.0	6.9	46.9	[32]

BT	37.8	37.5	75.4	[33]
PC	44.6	3.6	48.2	[34]
MWCNT	18.4	26.9	45.3	[30],[35]

Most common polymers with surface energy in the range of 20-40 mN.m^{-1}[36] are considered as low surface energy materials. However, from the data in Table 2, the surface energy values for PHP (46.9 mN m^{-1}) and PC (48.2 mN m^{-1}) are obviously higher than the given range. Therefore, the difference between surface energies for the components of PHP/PC/BT and PHP/PC/MWCNT nanocomposites were calculated based on the Owens-Wendt equation. The results indicate that for PHP/PC/BT system, the wetting coefficient is equal to -8.9 therefore the model predicts that the BT nanoparticles locate in PHP. Similarly, the wetting coefficient for PHP/PC/MWCNT system is less than -1, anticipating that the MWCNTs are localized in PHP.

3.2. Rheological Measurements

Frequency sweep measurements were done to get insight into the viscosity of the polymer melts at relevant processing conditions. By knowing the viscosity ratio of the binary polymer blends (η_2/η_1) at the processing condition, the volume fraction ($\theta_2/\ \theta_1$) at which the phase inversion occurs is predictable by equation 6 known as Wu's semi-empirical equation.[37]

$$\frac{\theta_2}{\theta_1} = 1.22\left(\frac{\eta_2}{\eta_1}\right)^{0.29} \qquad \text{(Eq. 6)}$$

In the applied frequency range, PC viscosity is almost stable while PHP shows a shear thinning behavior. By measuring the viscosity of PHP and PC at processing conditions; 250°C and 150 rpm, which is marked by star on the viscosity plot in Figure 2, it is predicted that the phase inversion occurs at θ_{PC}=37 vol% and θ_{PHP}=63 vol% equal to 28 wt.% of PC.

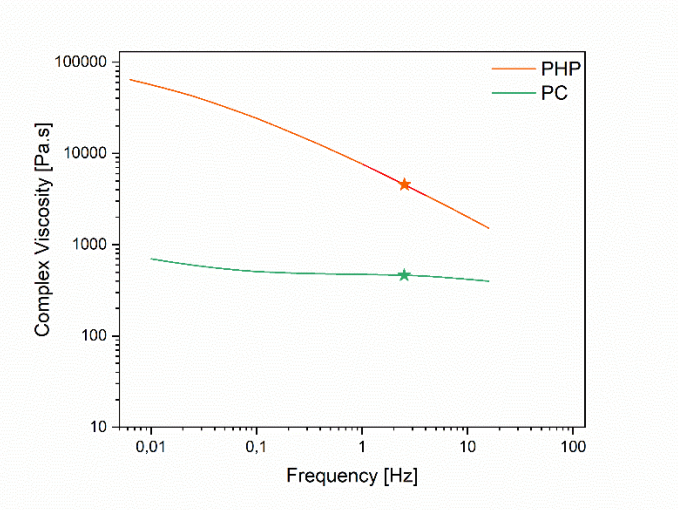

Figure 2. Frequency dependence of complex viscosity for pristine PHP and PC at 250°C

3.3. Morphology studies and selective localization of nanofillers

The developed polymer blend nanocomposites can form various morphologies, depending on rheological properties, interfacial tension between the components, blending conditions and blend composition.[38] In this regard, PHP/PC blends were fabricated at the same processing conditions but different weight ratios and BT and/or MWCNT were embedded in the polymer blends to investigate the effects of blend ratio and nanofillers selective localization on morphology evolution. Figure 3a and 3e illustrate the fractured surfaces of 90/10/0/0 and 70/30/0/0 PVDF/PC blends in which PC formed spherical domains and the border between the two phases are clearly seen indicating that a matrix-droplet morphology is formed. It is observed that the 90/10/0/0 blend has a fine morphology while with increasing the blend ratio to 70/30/0/0 large droplets are formed suggesting that the interfacial interactions between the phases are weak. As discussed in the rheological studies, PC has lower viscosity than PHP at the processing conditions. Thereby, during the simultaneous coalescence and dispersion of the polymers in melt mixing, the coalescence occurs faster for the PC.

Selective localization of nanofillers is an attractive approach to tailor morphology and modify final properties of the polymer blends for the application of interest. Figure 3b and 3f exhibit that in 90/10/3/0 and 70/30/3/0 nanocomposites, BTs are fairly dispersed in the PHP matrix without formation of large agglomerations while some of them are placed at the

interphase and on the surface of polycarbonate. For the sake of clarity, the images at higher magnifications are presented at Figure 4a and 4b. As shown in Figure 3c, the MWCNTs are located at the PC phase of 90/10/0/3 nanocomposite and presence of MWCNTs transformed the PC domains to deformed spherical inclusions. Figure 4c and 4f confirm this localization at higher magnifications. It is also visible that the interface of ternary nanocomposites became more blurred because by addition of the BT or MWCNT nanofillers, a higher shear stress is applied to the polymer melts so that the dispersion quality of the polymers improves and a finer morphology is achieved. Moreover, selective localization of fillers in PC and the interphase adjusts the melt viscosity ratio between the components and hampers the coalescence of this phase assisting formation of a more uniform structure.[39] An interesting observation in Figure 3d is that the simultaneous presence of BT and MWCNT in 90/10/1.5/1.5 decreased the domains size substantially compared to the ternary 90/10/0/3 or 90/10/3/0 nanocomposites.

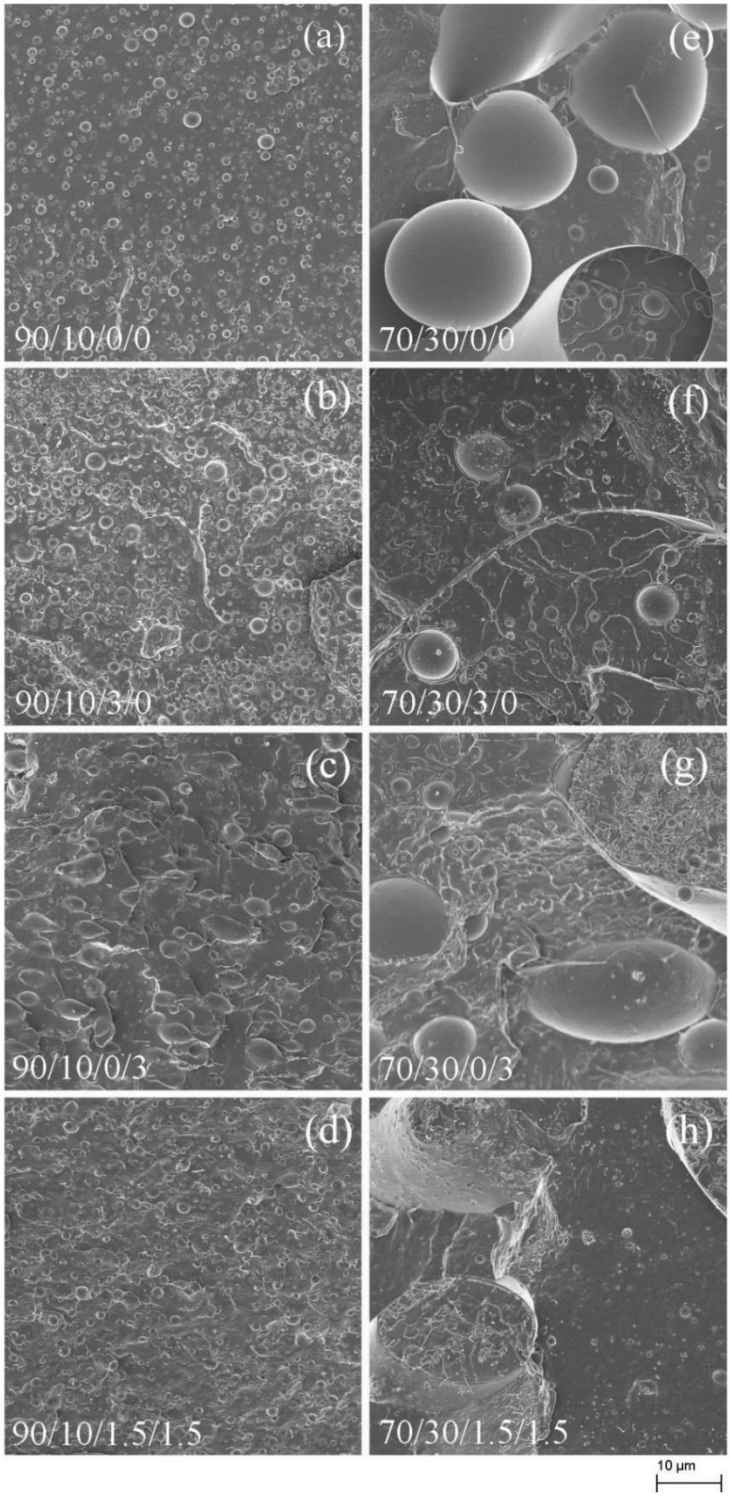

Figure 3. SEM micrographs of (a, e) PHP/PC blends, (b, f) PHP/PC/BT, (c, g) PHP/PC/MWCNT and (d, h) PHP/PC/BT/MWCNT nanocomposites

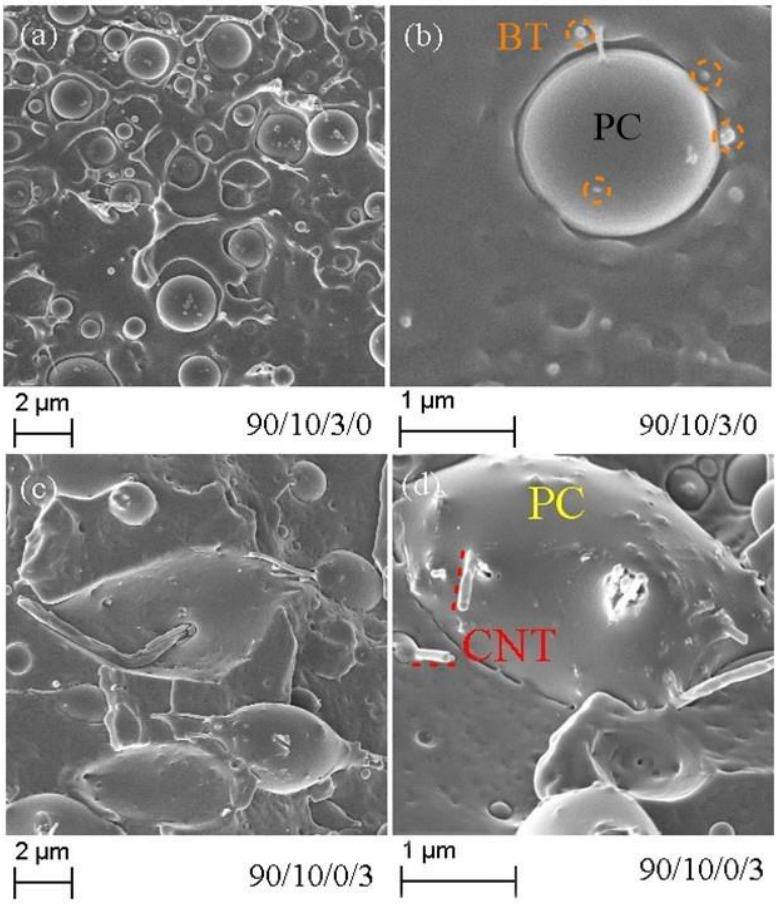

Figure 4. SEM micrographs of (a, b) 90/10/3/0 and (c, d) 90/10/0/3 at different magnifications

Figure 5 shows the TEM images of the 90/10/1.5/1.5 nanocomposite at 2 μm and 500 nm scales. The measured mean diameter of BT nanoparticles is 94 nm which is in agreement with the reported value by manufacturer. As predicted by theoretical models, BT nanoparticles are localized in PHP phase; however, it can be seen in Figure 5a, 5b, 5c and 5d that some of them are located at the interphase of PHP and PC in order to modulate viscosity ratio and reduce the interfacial energy differences. Also, it is clearly seen that unlike Owens Wendt equation prediction, the MWCNTs are found at the interphase (Figure 5b and 5c) and PC phase (Figure 5d). Interestingly, MWCNTs are dispersed individually without formation of any agglomerations. Figure 6 presents the TEM images of 70/30/1.5/1.5 nanocomposites. In the same manner, the BT nanoparticles are dispersed in the PHP phase with some degrees of localization at the interphase and the MWCNTs are settled in the PC phase. Consequently, the theoretical predictions were almost valid about BT but not about MWCNT. One possible explanation for this observation is that most of the calculations for

predicting nanofiller localization in ternary systems are conducted at room temperature although the surface energies at processing temperature are different.[29] To have more accuracy in nanofiller prediction, there are proposed expressions like Guggenheim's or thermal coefficients to extrapolate the surface energies of the polymers to the processing temperature but these data are limited in most cases which may affect the accuracy of the predictions. Another reason is that aside from thermodynamic affinity of filler and polymer, kinetic factors such as melt viscosity ratio and processing conditions such as mixing time, shear strength, and sequence of incorporation also affect the preferred location of the fillers in binary polymer systems. Wu et al. investigated selective localization of CNT and clay on morphology evolution of PCL/PLA blend matrixes. The samples were prepared by melt mixing at 70/30 or 30/70 wt.% of polymers, followed by compression molding. They found that clay is mostly localized at PLA while CNT is mainly found in PCL. In this study also, a deviation from theoretical prediction is observed about CNT; the geometric-mean equation predicted that CNT will be found in the PLA phase while TEM results depicted that they are placed in PCL. Herein, the competitive role between the thermodynamic aspects and kinetic effects such as viscosity ratio is shown; when the viscosity ratio is high, CNT tends to localize in PCL with lower viscosity but when the viscosity ratio is reduced, the thermodynamic aspects become dominant and CNT disperses in PLA.[31]

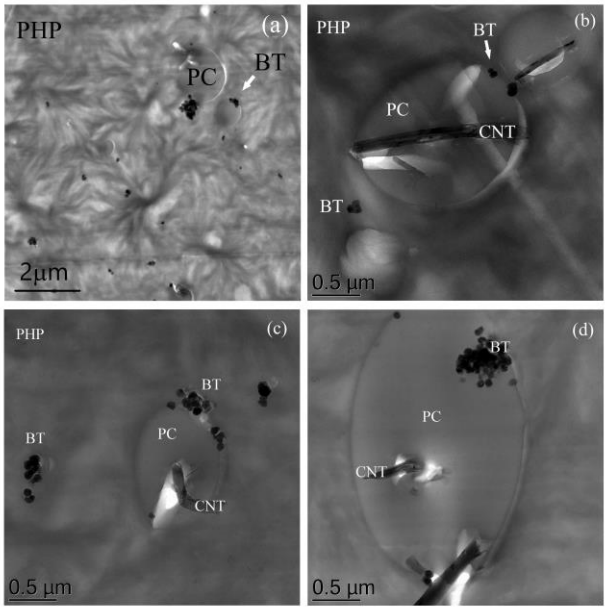

Figure 5. (a) Cross-section TEM image of 90/10/1.5/1.5 nanocomposite, (b, c, d) local view of image (a)

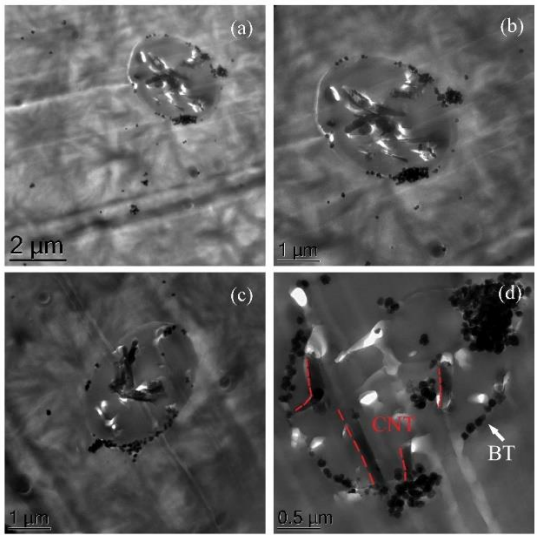

Figure 6. (a) Cross-section TEM image of 70/30/1.5/1.5 nanocomposite, (b, c, d) local view of image (a)

3.4. Characterization of the structure

FTIR spectroscopy was employed to investigate the crystalline structure of pure PHP and the effect of blending, adding BT and/or MWCNT nanoparticles and their synergistic effect on the β electroactive phase content. FTIR spectra in Figure 7 depicts PHP characteristic peaks related to the amorphous phase at 870 cm^{-1},[40] the α crystalline phase at 485, 531, 614, 762, 795, 974 cm^{-1} and the β crystalline phase at 510, 840 and 1279 cm^{-1}.[41] γ characteristic peaks[5] were not observed in the PHP revealing that the structure is only comprised of α and β phases.

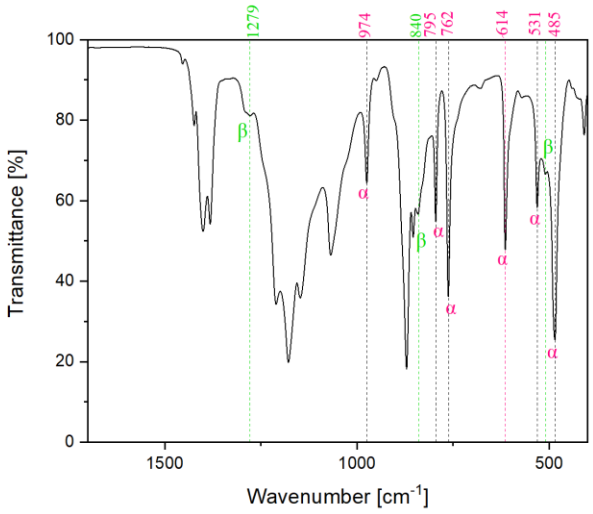

Figure 7. FTIR spectra of pure PHP

It can be seen from the graphs in Figure 8 that the β characteristic peak at 840 cm^{-1} is almost unchanged in all nanocomposites whereas the α phase fingerprint intensities decreased considerably meaning that the α phase suppressed as such β/α ratio increased. This finding is consistent with those of previous studies which found that addition of BT nanoparticles decreased α related peaks in PVDF/BT nanocomposites. The strong interaction between positively charged $–CH_2$ groups of PVDF and negatively charged surface of BT along with alignment of the chains on the surface of the nanoparticles alters the conformation to the extended all trance, promoting the crystal formation of β-phase.[13]

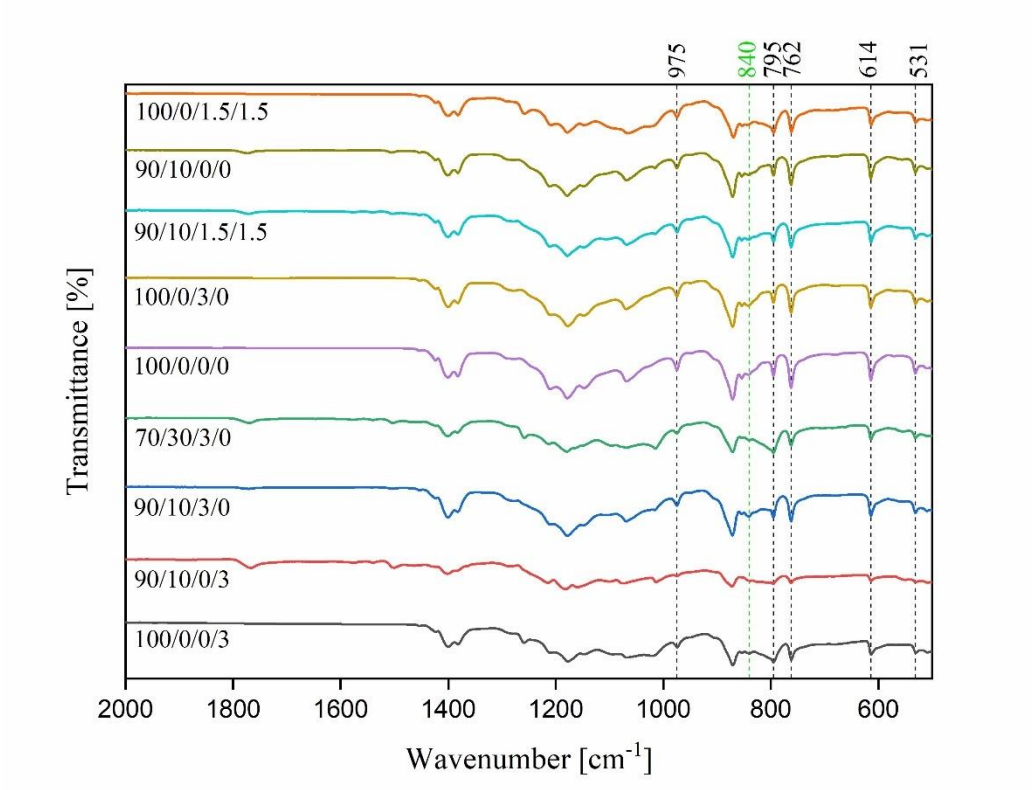

Figure 8. FTIR spectrum of PHP, PC, and their blends and nanocomposites

Besides qualitative analysis of the crystalline forms in the structure, FTIR can be used for quantitative analysis of the electroactive phase content. The fraction of β phase in the structure containing only α and β phases can be calculated based on equation 7 in which F(β) represents β phase content, A_α and A_β are the absorbance at 762 and 840 cm^{-1} and $K_\alpha = 6.1\times10^4$, $K_\beta = 7.7\times10^4$ cm^2mol^{-1} represent absorption coefficients at these wavenumbers.[42]

$$F(\beta) = \frac{A_\beta}{(K_\beta / K_\alpha)A_\alpha + A_\beta} \quad \text{(Eq. 7)}$$

The FTIR spectroscopy was repeated three times for each sample and the average values are presented in the Table 3. As it can be seen from the data in this table, the β content is 35% for the pure PHP which interestingly increased to 39.1% by adding 3 wt. % BT and more efficaciously to 40.71% by incorporating 3 wt.% of MWCNTs. The simultaneous presence of BT and MWCNT in 100/0/1.5/1.5 nanocomposite increased the β content to 39.64 demonstrating the β induction clearly; however, the expected synergistic effect is not observed compared to the analogous 100/0/3/0 or 100/0/0/3 nanocomposites which may be due to the poor dispersion quality of nanofillers in the matrix or the low amount of BT used. The results are significant in the case of 90/10 blend nanocomposites either with 3 wt.% of BT or MWCNT where the fraction of the β phase reached 37.07% or 39.63%, respectively. The most striking result to emerge from the data in this table is the synergistic effect from the simultaneous presence of BT and MWCNT in the quaternary 90/10/1.5/1.5 nanocomposite which is attributed to the selective localization of BT and MWCNT nanofillers in the polymer blends, better dispersion quality of the nanofillers and the increased surface area at the interphase as discussed in SEM and TEM results.

Table 3. Determined contents of the β phase for the prepared samples

Sample	**F(β)%**	**Sample**	**F(β)%**
100/0/0/0	35.0 ± 0.29	**90/10/0/0**	34.4 ± 0.21
100/0/3/0	39.1 ± 0.22	**90/10/3/0**	37.1 ± 0.23
100/0/0/3	40.7 ± 0.28	**90/10/0/3**	39.6 ± 0.22
100/0/1.5/1.5	39.6 ± 0.18	**90/10/1.5/1.5**	39.1± 0.11

3.5. Crystallography of the structure

XRD measurements can usefully supplement the β content and crystallinity studies of the PHP nanocomposites. The results obtained for all nanocomposite systems are presented in Figure 9. PHP showed the characteristic peaks related to the α phase at 17.63° (100), 18.34°

(020), 19.86° (110) and 26.56° (021).[16],[28] The small peak appeared at 20.26° corresponds to the sum of diffractions of (110) and (200) planes of β phase.[5],[43] Addition of 3 wt.% BT to PHP (100/0/3/0) reduced all α peak intensities while the small peak appeared at 20.6° is assigned to β induction in the nanocomposite. Moreover, the peaks at 2θ= 22.0° (100), 31.4° (110), 38.8° (111), 45.0° (002) are ascribed to BT diffraction peaks[44],[45] which clearly demonstrates that BTs are fully filled in the polymer matrix. Incorporating MWCNT to the matrix decreased the α peaks at 17.63°, 18.34°, 19.86° while increased the peak intensity at 26.56° due to the overlap of α phase and MWCNT characteristic peaks. The observed shoulder at 20.6° is an indication of β induction and α restriction in 100/0/0/3 sample which supports previous researches.[46] It is already reported that zig-zag lattice structure of the MWCNT matches well with the all trans conformation of the β phase in PVDF resulting in stable bonding between them. In other words, MWCNTs act as nucleating agents promoting β−phase formation in the PVDF matrix.[47] The same trend is observed for 100/0/1.5/1.5 nanocomposites with α related peaks reduction and β shoulder formation. Additionally, the peak intensities related to BT is half of 100/0/3/0 nanocomposite.

After blending PHP with PC (90/10/0/0), the intensity of the α phase characteristic peaks decreased at 18.34° and 20.0° because of the amorphous nature of PC which is consistent with those of Chiu's studies.[28] The blend nanocomposites also showed a clear reduction in the α phase peak intensities. Interestingly, this trend is more pronounced for the 90/10/1.5/1.5 compared to the analogous ternary 90/10/3/0 and 90/10/0/3 nanocomposite.

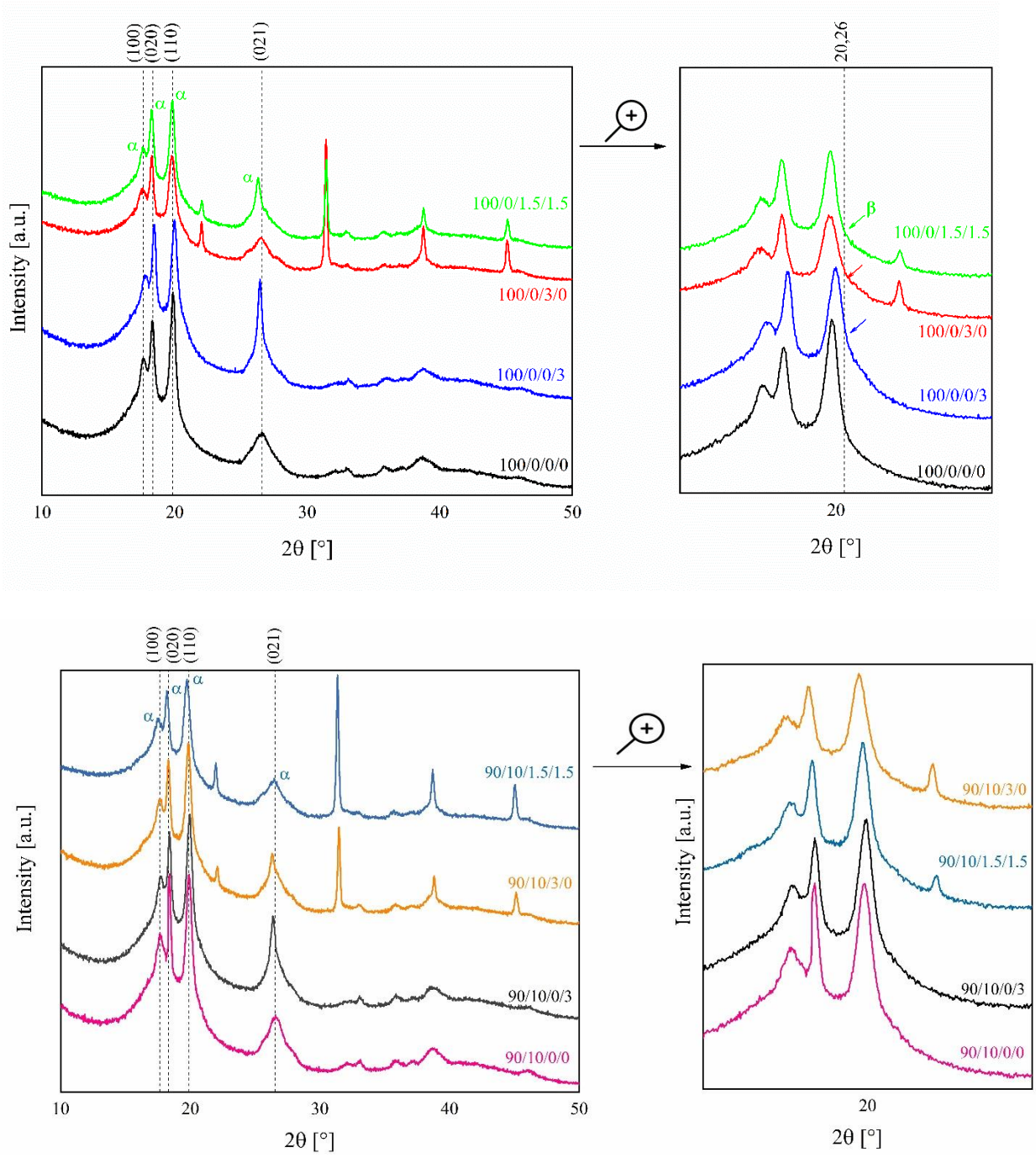

Figure 9. XRD diffractograms of crystalline PHP and 90/10 blend nanocomposites

The DSC curves of PHP, PHP/PC blends and blend nanocomposites are shown in MWCNT is preferentially located in PC phase.

Figure 10a. Also, the thermal parameters derived from preliminary analysis of heating and cooling runs are summarized in Table 4. PHP shows melting temperature at about 155 °C.

Addition of nanofillers or blending did not change the melting temperature considerably but the enthalpy of fusion and the area under the melting curve. Decreased enthalpy of fusion for the samples indicates that addition of nanoparticles helped formation of more uniform crystals.

The results obtained from cooling runs are presented in MWCNT is preferentially located in PC phase.

Figure 10b. The crystallization temperature for the pure PHP is observed at 128.6 °C. Addition of 3 wt.% MWCNT to the system increased the T_c significantly indicating that the crystallization was facilitated and more chains were aligned on the nanoparticles surface resulting in β enhancement which is in agreement with FTIR results. It can be seen that the crystallization temperature of 90/10/0/3 and 70/30/0/3 are almost unchanged compared to

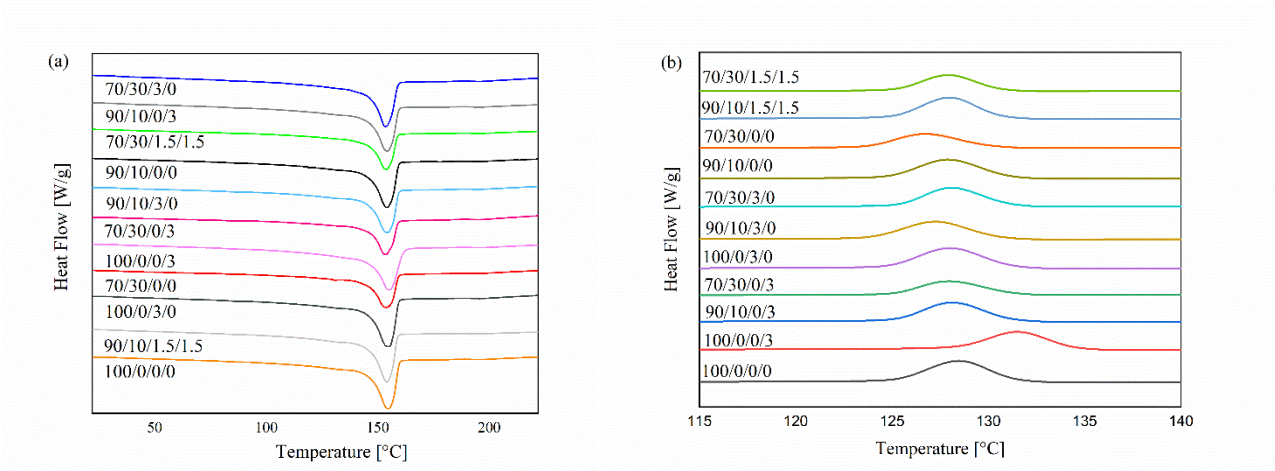

the neat PHP revealing that the MWCNT is preferentially located in PC phase.

Figure 10. DSC (a) heating and (b) cooling curves for pure PHP and nanocomposites

Table 4. Melting and crystallization enthalpy and temperature and crystallinity degree of prepared samples

sample	ΔH_m (J/g)	ΔH_{PHP} (J/g)	ΔH_C (J/g)	T_m (°C)	T_c (°C)	X_c (%)
100/0/0/0	47.91	47.91	37.34	154.9	128.6	45.85
90/10/0/0	42.12	46.61	32.63	153.4	127.9	44.60
70/30/0/0	32.35	45.50	22.92	153.9	126.7	43.54

70/30/3/0	37.02	53.69	29.00	153.3	128.1	51.38
100/0/0/3	39.68	40.82	32.65	154.9	131.5	39.06
90/10/3/0	43.71	49.78	31.50	153.7	127.3	47.64
100/0/3/0	48.85	50.26	35.18	154.2	128.0	48.10
90/10/0/3	46.84	53.36	31.02	153.9	128.1	51.06
70/30/0/3	29.93	43.25	32.20	153.1	128.0	41.39
90/10/1.5/1.5	40.55	46.17	31.31	153.7	128.0	44.18
70/30/1.5/1.5	29.62	42.80	22.94	153.6	127.9	40.96

Crystallinity percentage was calculated based on equation 8

$$X_c\% = \frac{\Delta H_m}{w\Delta H_m^\circ} \times 100 \qquad \text{(Eq. 8)}$$

where ΔH_m is the measured melting enthalpy; the integrated areas under the curves, w is mass fraction of PHP and ΔH_m° is heat of fusion of 100% crystalline PHP which is equal to 104.5 J g^{-1}.[48] Polycarbonate showed an endothermic peak at about 140 °C therefore the melting enthalpy of the PHP was calculated according to equation 9.

$$\Delta H_{PHP} = \frac{\Delta H_{total} - \Delta H_{PC}(1 - w_{PHP})}{w_{PHP}} \qquad \text{(Eq. 9)}$$

The results obtained from crystallinity degree are summarized in Table 4 and rearranged from high to low in Figure 11 for ease of comparison. Blending PHP with amorphous polycarbonate reduced chain order and hence crystallinity which confirms FTIR and XRD results. Higher crystallinity degree in 90/10/3/0, 100/0/3/0, 90/10/0/3 and 70/30/3/0 is attributed to the nucleation effects of BT or MWCNT in the nanocomposites. PC may contain 1–2% crystallinity degree and loading MWCNT can increase the crystalline content of the polymer.[49] Higher crystallinity degree in 90/10/0/3 compared to 100/0/0/3 suggests that the MWCNTs are localized in PC which supports TEM observations.

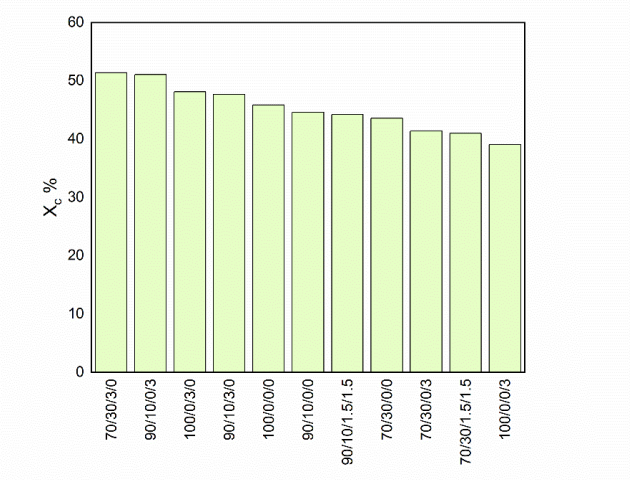

Figure 11. Crystallinity percentage for the investigated samples

4. Conclusion

This study has explained the central importance of combined ceramic BT and conductive MWCNT nanofillers on β content enhancement and morphology evolution in PHP/PC blends. PHP is thermodynamically favored phase for localization of BT and MWCNT, predicted by the geometric mean equation; however, SEM and TEM observations indicated that BT is mainly located within PHP and some of them are localized in the interphase while MWCNTs are settled in the PC and interphase. Accordingly, the selective localization and final distribution of nanofillers during melt mixing is not only determined by thermodynamic aspects and the affinity between filler-polymer, but also the kinetic aspects such as viscosity ratio of two components. The considerable reduction in domains size of 90/10/1.5/1.5 indicates that the nanofillers act as nano-reinforcements and compatibilizer simultaneously improving morphology and final properties in PHP/ PC blend. FTIR results confirmed the synergistic effects of BT and CNT in β induction in 90/10/1.5/1.5 nanocomposite compared to the ternary PHP/PC/BT and PHP/PC/MWCNT nanocomposites. Besides, XRD analysis depicted α phase suppression in all nanocomposites supporting FTIR results. DSC analysis shed light on positive nucleating effects of BT and MWCNT in the nanocomposites.

Reference

[1] Zhang, C.; Guo, Z.; Zheng, X.; Zhao, X.; Wang, H.; Liang, F.; Guan, S.; Wang, Y.; Zhao, Y.; Chen, A.; Zhu, G.; Wang, Z. L. *Adv. Mater.* **2020**, *32*, 1.

[2] Chen, A.; Zhang, C.; Zhu, G.; Wang, Z. L. *Adv. Sci.* **2020**, *7*, 2000186.

[3] Zhang, C.; Fan, Y.; Li, H.; Li, Y.; Zhang, L.; Cao, S.; Kuang, S.; Zhao, Y.; Chen, A.; Zhu, G.; Wang, Z. L. *ACS Nano* **2018**, *12*, 4803.

[4] Wang, X.; Sun, F.; Yin, G.; Wang, Y.; Liu, B.; Dong, M. *Sensors* **2018**, *18*, 330.

[5] Martins, P.; Lopes, A. C.; Lanceros-mendez, S. *Prog. Polym. Sci.* **2014**, *39*, 683.

[6] Roy, S.; Thakur, P.; Hoque, N. A.; Bagchi, B.; Das, S. *RSC Adv.* **2016**, *6*, 21881.

[7] Chen, J.; Wang, Y.; Yuan, Q.; Xu, X.; Niu, Y.; Wang, Q.; Wang, H. *Nano Energy* **2018**, *54*, 288.

[8] Kasbi, S. F.; Jafari, S. H.; Khonakdar, H. A.; Goodarzi, V.; Torabi, A. *J. Appl. Polym. Sci.* **2020**, *137*, 49403.

[9] Kumar, G. S.; Vishnupriya, D.; Joshi, A.; Datar, S.; Patro, T. U. *Phys. Chem. Chem. Phys.* **2015**, *17*, 20347.

[10] Abolhasani, M. M.; Shirvanimoghaddam, K.; Naebe, M. *Compos. Sci. Technol.* **2017**, *138*, 49.

[11] Gong, X.; Chen, Y.; Tang, C. Y.; Law, W. C.; Chen, L.; Wu, C.; Hu, T.; Tsui, G. C. P. *J. Appl. Polym. Sci.* **2018**, *135*, 2.

[12] Feng, Y.; Hou, Y. F. *J. Mater. Chem. C* **2015**, *3*, 1250.

[13] Jia, N.; Xing, Q.; Xia, G.; Sun, J.; Song, R.; Huang, W. *Mater. Lett.* **2015**, *139*, 212.

[14] Alluri, N. R.; Saravanakumar, B.; Kim, S. J. *ACS Appl. Mater. Interfaces* **2015**, *7*, 9831.

[15] Fu, J.; Hou, Y.; Zheng, M.; Wei, Q.; Zhu, M.; Yan, H. *ACS Appl. Mater. Interfaces* **2015**, *7*, 24480.

[16] Li, Y. C.; Tjong, S. C.; Li, R. K. Y. *Express Polym. Lett.* **2011**, *5*, 526.

[17] Zhou, L.; Fu, Q.; Xue, F.; Tang, X.; Zhou, D.; Tian, Y.; Wang, G.; Wang, C.; Gou, H.; Xu, L. *ACS Appl. Mater. Interfaces* **2017**, *9*, 40792.

[18] Jin, Y.; Xia, N.; Gerhardt, R. A. *Nano Energy* **2016**, *30*, 407.

[19] Fan, B.; Bedoui, F.; Weigand, S.; Bai, J. *J. Phys. Chem. C* **2016**, *120*, 9511.

[20] Tang, H.; Zhou, Z.; Sodano, H. A. *ACS Appl. Mater. Interfaces* **2014**, *6*, 5450.

[21] Ponnamma, D.; Al-Maadeed, M. A. A. *Sustain. Energy Fuels* **2019**, *3*, 774.

[22] Jin, S. H.; Choi, D. K.; Lee, D. S. *Colloids Surfaces A Physicochem. Eng. Asp.* **2008**, *313*, 242.

[23] Baudouin, A. C.; Devaux, J.; Bailly, C. *Polymer* **2010**, *51*, 1341.

[24] Zhou, Z.; MacKey, M.; Carr, J.; Zhu, L.; Flandin, L.; Baer, E. *J. Polym. Sci. Part B Polym. Phys.* **2012**, *50*, 993.

[25] Su, C.; Xu, L.; Zhang, C.; Zhu, J. *Compos. Sci. Technol.* **2011**, *71*, 1016.

[26] Biswas, S.; Kar, G. P.; Bose, S. *Phys. Chem. Chem. Phys.* **2015**, *17*, 27698.

[27] Chen, J.; Lu, H. yi; Yang, J. hui; Wang, Y.; Zheng, X. tong; Zhang, C. liang; Yuan, G. ping *Compos. Sci. Technol.* **2014**, *94*, 30.

[28] Chiu, F. C. *Polym. Test.* **2017**, *62*, 115.

[29] Fenouillot, F.; Cassagnau, P.; Majeste, J. *Polymer* **2009**, *50*, 1333.

[30] Göldel, A.; Kasaliwal, G.; Pötschke, P. *Macromol. Rapid Commun.* **2009**, *30*, 423.

[31] Wu, D.; Lin, D.; Zhang, J.; Zhou, W.; Zhang, M.; Zhang, Y.; Wang, D.; Lin, B. *Macromol. Chem. Phys.* **2011**, *212*, 613.

[32] Ganesh, V. A.; Nair, A. S.; Raut, H. K.; Tan, T. T. Y.; He, C.; Ramakrishna, S.; Xu, J. *J. Mater. Chem.* **2012**, *22*, 18479.

[33] Su, J.; Zhang, J. *Appl. Surf. Sci.* **2016**, *388*, 531.

[34] Terpilowski, K.; Rymuszka, D.; Holysz, L.; Chibowski, E. In *Proceedings of the 8th International Conference MMT-20142, Ariel, Israel*; **2014**, *28*,155.

[35] Nuriel, S.; Liu, L.; Barber, A. H.; Wagner, H. D. *Chem. Phys. Lett.* **2005**, *404*, 263.

[36] Verkuijlen, R. O. F.; Dongen, M. H. A. Van; Stevens, A. A. E.; Geldrop, J. Van; Bernards, J. P. C. *Appl. Surf. Sci.* **2014**, *290*, 381.

[37] Moussaif, N.; Jérôme, R. *Polymer* **1999**, *40*, 3919.

[38] Hoseini, A. H. A.; Arjmand, M.; Sundararaj, U.; Trifkovic, M. *Eur. Polym. J.* **2017**, *95*, 418.

[39] Liebscher, M.; Tzounis, L.; Pötschke, P.; Heinrich, G. *Polymer* **2013**, *54*, 6801.

[40] Peng, G.; Zhao, X.; Zhan, Z.; Ci, S.; Wang, Q.; Liang, Y.; Zhao, M. *RSC Adv.* **2014**, *4*, 16849.

[41] Singh, V. K.; Singh, R. K. *J. Mater. Chem. C* **2015**, *3*, 7305.

[42] Ponnamma, D.; Al-Maadeed, M. A. A. *Sustain. energy fuels* **2019**, *3*, 774.

[43] Sabry, R. S.; Hussein, A. D. *Polym. Test.* **2019**, *79*, 106001.

[44] Chen, X.; Li, X.; Shao, J.; An, N.; Tian, H.; Wang, C.; Han, T.; Wang, L.; Lu, B. *Small* **2017**, *13*, 1604245.

[45] Feng, Y.; Li, W. L.; Hou, Y. F.; Yu, Y.; Cao, W. P.; Zhang, T. D.; Fei, W. D. *J. Mater. Chem. C* **2015**, *3*, 1250.

[46] Varghese, S.; Eggedi, O.; Valiyaneerilakkal, U.; Darla, M. R.; Varghese, S. *AIP Adv.* **2014**, *4*, 47102.

[47] Laird, E. D.; Li, C. Y. *Macromolecules* **2013**, *46*, 2877.

[48] Roy, S.; Thakur, P.; Hoque, N. A.; Bagchi, B.; Das, S. *RSC Adv.* **2016**, *6*, 21881.

[49] Larosa, C.; Patra, N.; Salerno, M.; Mikac, L.; Meri, R. M.; Ivanda, M. *Beilstein J. Nanotechnol.* **2017**, *8*, 2026.